

A perturbative formalism for electronic transitions through conical intersections in a fully quadratic vibronic model

Julia S. Endicott,^{1,2} Loïc Joubert-Doriot,^{1,2} and Artur F. Izmaylov^{1,2}

¹⁾ *Department of Physical and Environmental Sciences, University of Toronto Scarborough, Toronto, Ontario, M1C 1A4, Canada*

²⁾ *Chemical Physics Theory Group, Department of Chemistry, University of Toronto, Toronto, Ontario, M5S 3H6, Canada*

(Dated: 16 January 2022)

We consider a fully quadratic vibronic model Hamiltonian for studying photoinduced electronic transitions through conical intersections. Using a second order perturbative approximation for diabatic couplings we derive an analytical expression for the time evolution of electronic populations at a given temperature. This formalism extends upon a previously developed perturbative technique for a linear vibronic coupling Hamiltonian. The advantage of the quadratic model Hamiltonian is that it allows one to use separate quadratic representations for potential energy surfaces of different electronic states and a more flexible representation of interstate couplings. We explore features introduced by the quadratic Hamiltonian in a series of 2D models, and then apply our formalism to the 2,6-bis(methylene) adamantyl cation, and its dimethyl derivative. The Hamiltonian parameters for the molecular systems have been obtained from electronic structure calculations followed by a diabatization procedure. The evolution of electronic populations in the molecular systems using the perturbative formalism shows a good agreement with that from variational quantum dynamics.

I. INTRODUCTION

Photoinduced charge, proton, and energy transfers are quite common processes in many areas of biological^{1–3} and technological^{4–6} significance. An adequate description of these processes requires inclusion of multiple electronic states and thus goes beyond the Born-Oppenheimer approximation. Potential energy surfaces (PESs) of electronic states in large systems quite commonly intersect forming conical intersections (CIs)^{7,8} which provide an efficient channel for energy redistribution via non-adiabatic dynamics.^{9,10} Generally, to account for quantum effects associated with non-adiabatic dynamics requires using methods of quantum dynamics whose computational cost scales exponentially with the number of degrees of freedom (DOF).¹¹ Mixed quantum-classical approaches^{12–15} partially alleviate the problem by treating nuclear dynamics with classical mechanics and employing quantum consideration to accommodate non-adiabatic transitions. However, application of these approaches can also be computationally demanding if one accounts for increasing number of classical trajectories needed for adequate sampling of quantum transitions and computational cost of electronic PES calculations associated with each trajectory.

For practical purposes though, one does not need to know dynamics of all DOF in a large system undergoing charge or energy transfer. In many cases the main interest is in properties related to only the electronic DOF: rates of electronic transitions or electronic state population dynamics. However, one cannot simply disregard nuclear DOF because their dynamics is the main cause of electronic transitions in the non-adiabatic dynamics. Instead, at least in semi-rigid systems, one can parametrize the nuclear DOF with a simple exactly solvable harmonic model and couple its nuclear dynamics in an analytic

form with electronic DOF through electron-nuclear couplings treated perturbatively in the spirit of the Marcus and Förster theories.^{16,17} Such perturbative treatment results in effective time-dependent electron transition rates that originate from the nuclear motion and define the electronic dynamics. Using the exactly solvable model for the nuclear dynamics makes these transition rates amenable to analytical treatment and thus removes the burden of the numerical propagation of the nuclear DOF completely.

These ideas have been implemented recently in the so-called non-equilibrium Fermi golden rule (NFGR)¹⁸ and generalized master equation approaches¹⁹ for CIs of two electronic states parametrized within the linear vibronic coupling (LVC) model Hamiltonian^{20–22}

$$H_{\text{LVC}} = \sum_{i=1}^N \begin{pmatrix} (p_i^2 + \Omega_i^2 q_i^2)/2 & 0 \\ 0 & (p_i^2 + \Omega_i^2 q_i^2)/2 + \Delta E \end{pmatrix} + \begin{pmatrix} d_{D,i} q_i & c_i q_i \\ c_i q_i & d_{A,i} q_i \end{pmatrix}. \quad (1)$$

H_{LVC} represents coupled donor and acceptor diabatic states by N -dimensional harmonic oscillators with frequencies Ω_i , mass weighted coordinates q_i and corresponding momenta p_i . Although the surfaces have the same frequencies they have different linear shifts, $d_{D,i} \neq d_{A,i}$, and are energetically separated by ΔE . The surfaces are coupled by linear coupling terms $c_i q_i$ that give rise to the CI topology in the adiabatic representation.

Assuming only constant shift differences $x_{G,i}$ between minima of the donor state and some ground electronic state with the Hamiltonian

$$\tilde{H}_G = \sum_{i=1}^N \frac{1}{2} [p_i^2 + \Omega_i^2 (q_i + x_{G,i})^2] \quad (2)$$

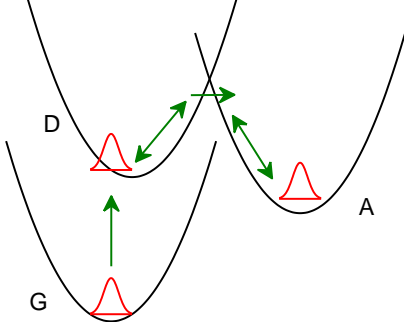


FIG. 1. Photo-induced non-radiative transition through a conical intersection.

using the NFGR approach one can study non-equilibrium electronic population dynamics when an initial ultra-fast laser pulse excites a ground state Boltzmann density to the donor state and then the electronic population is transferred to the acceptor state via non-radiative transition through a CI (see Fig. 1). As a limiting case of the zero shift between the ground and donor states the NFGR formalism can also be applied to model radiationless transfer starting with the equilibrium Boltzmann density on the donor state. Using the NFGR approach the electronic population dynamics of excited states were calculated for some test molecules and showed quantitative agreement for short times and qualitative agreement for longer times when compared to results of variational wave packet techniques.¹⁸

The assumption of the same frequencies and normal modes for the ground, donor, and acceptor states limits the applicability of the NFGR method. An extension of the LVC Hamiltonian, which is more general and allows the inclusion of effects such as the Duschinsky rotation²³ of the normal coordinates and changes in vibrational frequencies between two states, is the quadratic vibronic coupling (QVC) model Hamiltonian

$$H_{\text{QVC}} = \begin{pmatrix} H_D & V_{DA} \\ V_{AD} & H_A \end{pmatrix}, \quad (3)$$

$$H_D = \sum_{i=1}^N \frac{1}{2} p_{D,i}^2 + \frac{1}{2} \Omega_{D,i}^2 q_{D,i}^2, \quad (4)$$

$$H_A = \sum_{i=1}^N \frac{1}{2} p_{A,i}^2 + \frac{1}{2} \Omega_{A,i}^2 q_{A,i}^2 + \Delta E, \quad (5)$$

$$V_{DA} = V_{AD} = \sum_{i,j=1}^N \Theta_{ij} q_{D,i} q_{D,j} + \sum_{i=1}^N \gamma_i q_{D,i} + \Delta_{DA}, \quad (6)$$

where harmonic frequencies of the donor $\Omega_{D,i}$ and acceptor $\Omega_{A,i}$ states can be different, and normal modes of the acceptor state $q_{A,i}$ can be written as shifted and rotated

normal modes of the donor state $q_{D,i}$

$$q_{A,i} = \sum_{j=1}^N J_{ij}^{(A)} (q_{D,j} + x_{A,j}). \quad (7)$$

Here we introduced the unitary Duschinsky matrix $J_{ij}^{(A)}$ and the shift vector $x_{A,j}$ between the minima of the acceptor and donor states. Using the Duschinsky matrix, a Hessian matrix of the acceptor state can be written in terms of the donor normal modes as $\Omega'_A = \mathbf{J}^{(A)\dagger} \Omega_A \mathbf{J}^{(A)}$. H_{QVC} also differs from H_{LVC} by quadratic ($\Theta_{ij} q_{D,i} q_{D,j}$), and constant (Δ_{DA}) terms in the coupling potentials V_{DA} and V_{AD} . Picconi *et al.*²⁴ showed that using the QVC model rather than the LVC model can cause significant changes to both calculated spectra and electronic population dynamics in thymine. The QVC Hamiltonian with only a constant interstate coupling $V_{DA} = V_{AD} = \Delta_{DA}$ have been considered by Borrelli *et al.*,²⁵ however, this set up cannot result in the CI topology. As has been repeatedly shown, ignoring topological features of the CI can lead to qualitatively different predictions for nuclear dynamics.^{26–28}

Building the QVC Hamiltonian from *ab initio* electronic structure calculations is not a straightforward task because these calculations provide the adiabatic picture while the QVC Hamiltonian is written in the diabatic representation. The exact diabatic representation is impossible in practice for systems with more than one DOF,²⁹ and therefore, here we use approximate, so-called regularized diabatic states proposed by Köppel and coworkers.^{30,31} Construction of these states is based on removing only leading terms of non-adiabatic couplings that cause singularities at the CI seam. This removable part involves only states which participate in the CI, thus it is possible to rotate adiabatic states into regularized diabatic states where the singularities disappear.

In this paper we focus on extending the NFGR approach to the QVC Hamiltonian. To illustrate efficiency and accuracy of the developed approach we investigate internal electron transfer in the 2,6-bis(methylene)-adamantyl (BMA) and 2-methylene-6-isopropylidene-adamantyl (MIA) cations and compare our results to those obtained using the variational multiconfiguration Gaussian (vMCG)³² and multiconfiguration time dependant Hartree (MCTDH)³³ methods.

The rest of the paper is organized as follows. Section II provides main steps in the derivation of the central equation used to calculate evolution of the electronic donor state population, while further details are given in the Appendix. Section III uses 2D models and parametrized BMA and MIA model Hamiltonians to explore the capabilities of the NFGR method. Finally, Section IV concludes and provides an outlook for future work. Atomic units are used throughout this paper.

II. METHOD

For the QVC Hamiltonian [Eq. (3)] the electronic population of the donor diabatic state $|D\rangle$ can be written as a projection of the full electron-nuclear density on the donor state traced over all nuclear DOF,

$$P_D(t) = \text{Tr}_n [\langle D | e^{-iH_{\text{QVC}}t} \rho(0) e^{iH_{\text{QVC}}t} | D \rangle]. \quad (8)$$

To treat the quantum propagator $e^{-iH_{\text{QVC}}t}$ we employ a perturbation theory expansion by splitting the H_{QVC} Hamiltonian as

$$H_{\text{QVC}} = H_0 + V, \quad (9)$$

with

$$H_0 = |D\rangle\langle D| H_D + |A\rangle\langle A| H_A, \quad (10)$$

$$V = |D\rangle\langle A| V_{DA} + |A\rangle\langle D| V_{AD}, \quad (11)$$

where H_D , H_A , V_{DA} , and V_{AD} are given by Eqs. (3-6). The perturbative expansion of the propagator in the interaction picture up to the second order in V gives the evolution operator

$$U(t) = 1 - \int_0^t dt' \int_0^{t'} dt'' e^{iH_0 t'} V e^{-iH_0(t'-t'')} V e^{-iH_0 t''}. \quad (12)$$

Assuming an ultrafast laser pulse that promotes the ground state density $|G\rangle \rho_n \langle G|$ to the initial density on the donor state $\rho(0) = |D\rangle \rho_n(0) \langle D|$ and using the perturbative evolution operator $U(t)$ for the propagator, the equation for the donor state population becomes

$$\tilde{P}_D^{(2)}(t) = \text{Tr}_n [\langle D | U(t) | D \rangle \rho_n(0) \langle D | U^\dagger(t) | D \rangle]. \quad (13)$$

We further simplify Eq. (13) by excluding all terms of higher than the 2nd order in V and introducing $\rho_n(0) = e^{-\beta H_G} / \text{Tr}[e^{-\beta H_G}]$ as a Boltzmann distribution of the ground state with inverse temperature $\beta = 1/(k_B T)$

$$P_D^{(2)}(t) = 1 - 2\text{Re} \int_0^t dt' \int_0^{t'} dt'' f(t', t''), \quad (14)$$

where the time-correlation function $f(t', t'')$ is

$$f(t', t'') = \frac{1}{\text{Tr}_n[e^{-\beta H_G}]} \text{Tr}_n \left[e^{-\beta H_G} e^{iH_D t'} \times V_{DA} e^{-iH_A(t'-t'')} V_{AD} e^{-iH_D t''} \right]. \quad (15)$$

Here, the ground state Hamiltonian H_G is defined in a more general form than in the LVC consideration [cf. Eq. (2)]

$$H_G = \sum_{i=1}^N \frac{1}{2} p_{G,i}^2 + \frac{1}{2} \Omega_{G,i}^2 q_{G,i}^2, \quad (16)$$

$$q_{G,i} = \sum_{j=1}^N J_{ij}^{(G)} (q_{D,j} + x_{G,j}), \quad (17)$$

where $q_{G,i}$ are corresponding normal modes that are generally rotated by $J_{ij}^{(G)}$ and shifted by $x_{G,j}$ with respect to the donor normal modes.

Analytical form of the $f(t', t'')$ function is obtained using Gaussian integration for the traces in Eq. (15), details of the derivation can be found in the Appendix. The $f(t', t'')$ function contains all parameters of the H_{QVC} and H_G Hamiltonians as well as temperature of the initial Boltzmann distribution. Although the explicit form of the $f(t', t'')$ function is very lengthy (see the Appendix), this function encompasses a few essential factors for the electronic population dynamics: (1) couplings between vibrational levels of the donor and acceptor states, (2) zeroth order energy differences between interacting vibrational levels, (3) initial conditions of the nuclear distribution. A significant role in modulating the couplings between the vibrational levels is played by the corresponding Franck-Condon (FC) overlaps between the associated nuclear wave-functions. Due to an exponential dependence on the distance between the donor-acceptor minima the FC overlap influence usually overpowers that of the polynomial terms from the V_{DA} potential.

If vibrational levels of uncoupled donor and acceptor states become close in energy the population calculated using Eq. (14) becomes negative at longer times. To avoid this unphysical behaviour we perform a partial infinite resummation of the perturbative population expansion using the corresponding cumulant expansion.¹⁸ In the second order, the cumulant expansion amounts to exponentiating the second term in Eq. (14)

$$P_D^{[2]}(t) = e^{-2\text{Re} \left[\int_0^t dt' \int_0^{t'} dt'' f(t', t'') \right]}. \quad (18)$$

Using the analytical expression for the $f(t', t'')$ function evaluating the electronic population dynamics in Eq. (18) requires only two-dimensional time integration that is done numerically. As a result the NFGR procedure scales quadratically with the number of time steps and cubically with the number of nuclear DOF due to matrix manipulations involved in the $f(t', t'')$ evaluation.

III. RESULTS AND DISCUSSIONS

A. 2D Model

First, we will illustrate properties of the NFGR approach applied to 2D H_{QVC} model Hamiltonians with various parameters. The parameters for our generic 2D model are given in Table I, we will use this system as our base and then explore some modifications of its parameters. The system consists of ground, donor, and acceptor states, which can have different minima, frequencies, and normal modes. Figure 2 shows PESs of the donor and acceptor states and the initial population density after excitation from the ground state. Our results will be compared to those of the exact quantum dynamics obtained using the split operator method.³⁴ In all NFGR

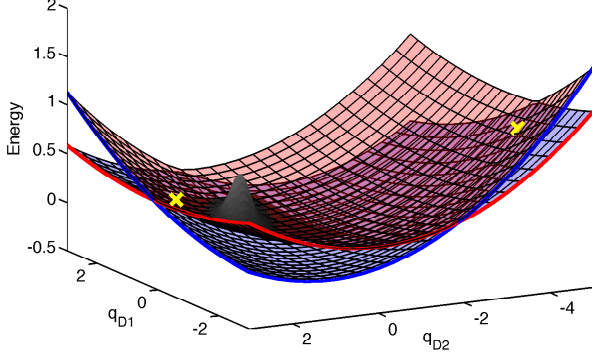


FIG. 2. Adiabatic PESs for the generic 2D model given in Table I. The lines at the edges of the plot show the diabatic states: the donor state in red and the acceptor state in blue. The crosses show the two conical intersections at $(-1.3, -4.4)$ and $(0.6, 2.2)$. The wave packet is a scaled version of the initial population density on the donor surface.

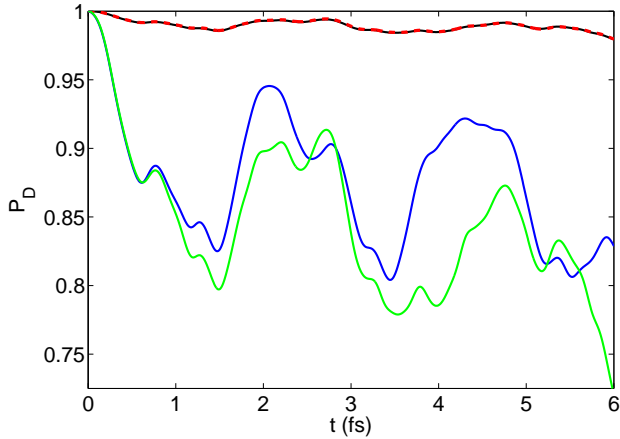


FIG. 3. Population dynamics using the exact and NFG approaches for the generic 2D model (Table I): exact (solid black) and NFG (dashed red); and for the strong coupling case (all couplings in Table I are enhanced 4 times): exact (solid blue), NFG (green).

simulations temperature is 2×10^{-8} a.u. (5×10^{-3} K), this makes values of β very large but finite and allows us to compare NFG simulations with those using the split operator approach at zero temperature.

In Fig. 3 the population of the donor state over time for the system given in Table I is shown for two cases: 1) the weak coupling case, where Θ , γ and Δ_{DA} are from Table I; and 2) the strong coupling case, where electronic coupling parameters Θ , γ and Δ_{DA} are four times those given in Table I. The weak coupling case shows excellent agreement between results of the exact and NFG methods. As expected for the perturbative approximation, in the strong coupling case, this agreement is quantitative only for short times but it remains qualitative for later

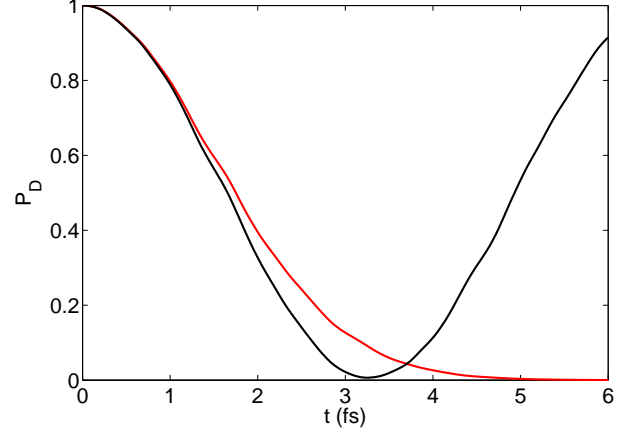


FIG. 4. Population dynamics for the generic 2D model (Table I) with modified parameters to satisfy the resonance condition $\Omega'_A = \begin{pmatrix} 0.2 & 0 \\ 0 & 0.3 \end{pmatrix}$, $\Delta E = 0$, and $\Delta_{DA} = 0.01$: exact (black) and NFG (red).

times.

The time-scale and extent of the donor-acceptor population transfer is highly dependant on the relative energies of the vibrational levels in each diabatic state. We will consider two cases: 1) when uncoupled vibrational levels of both diabates are energetically aligned, the resonant case; 2) when there is an energy difference between these levels, the non-resonant case. In the resonant case, the population of the donor state oscillates between 0 and 1 with a frequency that depends on the coupling strength. Fig. 4 illustrates that although the NFG approach does not capture coherent population oscillations it does reproduce accurately the time-scale of the forward donor-acceptor transfer. NFG does not account for the back transfer, and therefore it plateaus after the donor population depletion. Using a master equation framework³⁵ with NFG time-correlation functions [e.g., Eq. (23)] can partially alleviate this drawback.

In the non-resonant case, instead of the complete population transfer we observe only small amplitude population oscillations (see Fig. 3). With the LVC Hamiltonian model used in previous work¹⁸, the non-resonant regime could only appear due to the ΔE term. With the QVC model, the donor and acceptor states can have different frequencies and therefore be non-resonant for any ΔE . Figure 5 illustrates population oscillations arising from differences in donor-acceptor frequencies.

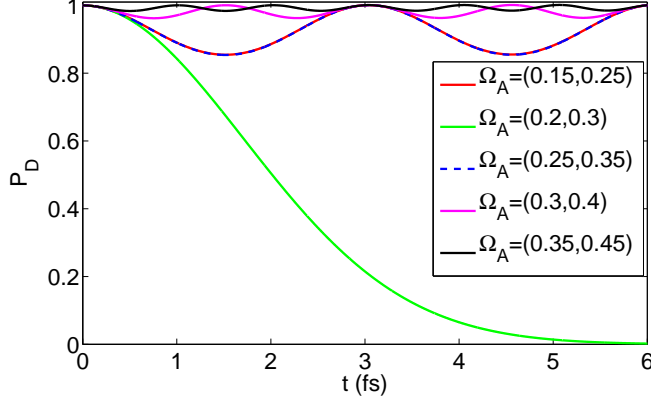
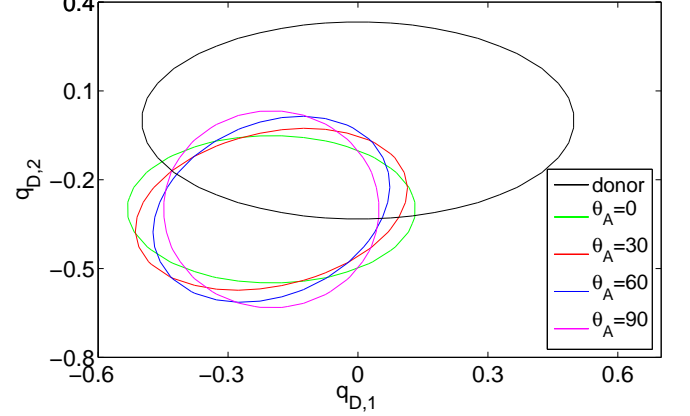
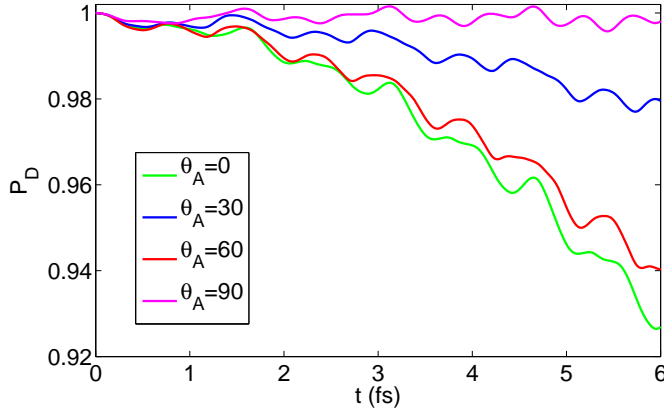
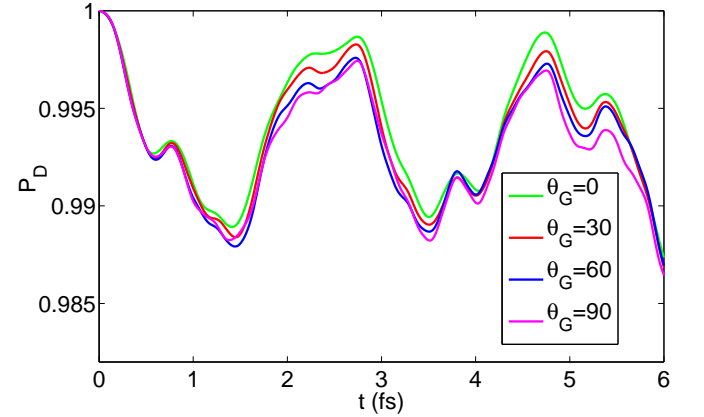
Using the QVC Hamiltonian, the NFG approach can also account for the rotation and translation of the vibrational normal modes of different electronic states (the Duschinsky effect). To study the effect of the Duschinsky rotation, we parametrized $\mathbf{J}^{(A)}$ and $\mathbf{J}^{(G)}$ matrices as

$$\mathbf{J}^{(S)} = \begin{pmatrix} \cos \theta_S & -\sin \theta_S \\ \sin \theta_S & \cos \theta_S \end{pmatrix}, \quad (19)$$

where S indicates the electronic state, and $\theta_A(\theta_G)$ is the angle between normal modes of the donor and accep-

TABLE I. Parameters for the generic 2D model.

Ω_D	Ω'_G, Ω'_A	\mathbf{x}_G	\mathbf{x}_A	Θ	γ	Δ_{DA}	ΔE
$\begin{pmatrix} 0.2 & 0.0 \\ 0.0 & 0.3 \end{pmatrix}$	$\begin{pmatrix} 0.2 & 0.1 \\ 0.1 & 0.3 \end{pmatrix}$	$\begin{pmatrix} -0.4 \\ -0.8 \end{pmatrix}$	$\begin{pmatrix} 0.2 \\ 0.3 \end{pmatrix}$	$\begin{pmatrix} 0.0002 & 0.0001 \\ 0.0001 & 0.0003 \end{pmatrix}$	$\begin{pmatrix} 0.003 \\ 0.001 \end{pmatrix}$	0.001	-0.2

FIG. 5. NFGR population dynamics for the 2D model with ΔE , Θ , γ , \mathbf{x}_G , and \mathbf{x}_A are all set to zero and $\Omega_G = \Omega_D = \begin{pmatrix} 0.2 & 0 \\ 0 & 0.3 \end{pmatrix}$, $\Delta_{DA}=0.01$ and Ω_A is diagonal and varied according to the legend.FIG. 7. Isoenergetic cross sections of the diabatic donor and acceptor PESs for 2D models with various values of the acceptor state rotation angle θ_A [Eq. (19)] and other parameters from Table I.FIG. 6. NFGR population dynamics for 2D models with different values of the acceptor state rotation angle θ_A [Eq. (19)] and other parameters from Table I.FIG. 8. NFGR population dynamics for 2D models with various values of the ground state rotation angle θ_G [Eq. (19)] and other parameters from Table I.

tor (ground) state. Figure 6 shows that the population transfer decreases with θ_A . This can be attributed to the reduction of FC overlaps between vibrational states of the donor and acceptor states with θ_A increase (see Fig. 7).

The Duschinsky rotation $\mathbf{J}^{(G)}$ also affects the population dynamics because the initial nuclear distribution is taken as a Boltzmann distribution of the ground state in Eq. (13) (see Figs. 8 and 9). The change in population transfer due to $\mathbf{J}^{(G)}$ is much smaller than that from $\mathbf{J}^{(A)}$ because the former does not affect coupling between

donor and acceptor states but only modifies initial conditions. Although the changes in population transfer with rotation of the ground state are small there is an overall trend of increased population transfer with ground state rotation in this system.

Besides rotations, the H_{QVC} Hamiltonian accounts for shifts between minima of different electronic states. Shifting the acceptor state minimum away from that of the donor state reduces the transfer as FC overlaps between donor and acceptor vibrational states decrease. Increasing the distance between the ground and donor state minima puts a non-equilibrium initial population distri-

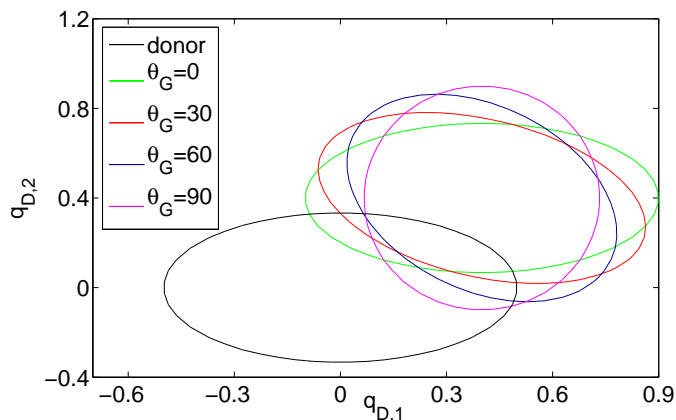


FIG. 9. Isoenergetic cross sections of the diabatic ground and donor PESs for 2D models with various values of the ground state rotation angle θ_G [Eq. (19)] and other parameters from Table I.

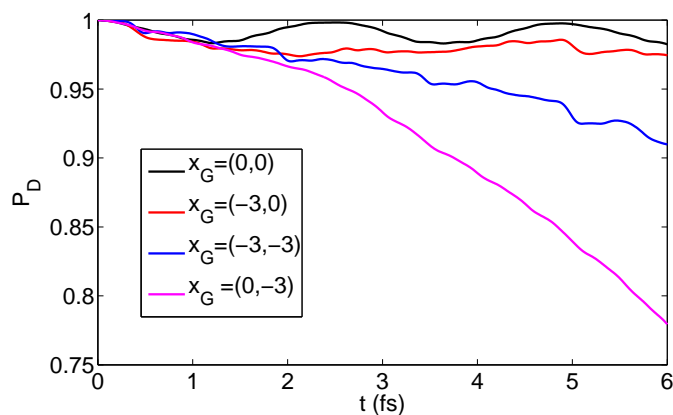


FIG. 10. NFGR population dynamics for 2D models with various values of the ground state shift x_G and other parameters from Table I.

bution higher on a slope of the donor diabatic state after vertical excitation from the minimum of the ground state. Figure 10 shows the electronic population dynamics for a series of systems with different ground state shifts. The generic model given in Table I has been modified for this part by making $q_{D,1}$ the coupling mode with $x_{A,1} = 0$, and $q_{D,2}$ the tuning mode with $\gamma_2 = \Theta_{2,2} = \Theta_{1,2} = \Theta_{2,1} = 0$. This modification allows us to separate the effect from shifting the ground state minimum along the tuning mode from that along the coupling mode. Shifting the ground state minimum along the coupling coordinate increases slightly the population transfer [$\mathbf{x}_G = (-3, 0)$ in Fig. 10]. It is expected because as the wave packet travels further along the coupling coordinate it spends more time in areas of higher coupling. Shifting the ground state minimum along the tuning coordinate increases drastically the population transfer [$\mathbf{x}_G = (0, -3)$ in Fig. 10]. This is consistent with the topography of the surfaces in Fig. 2, since in this case the wave packet oscillates between the two con-

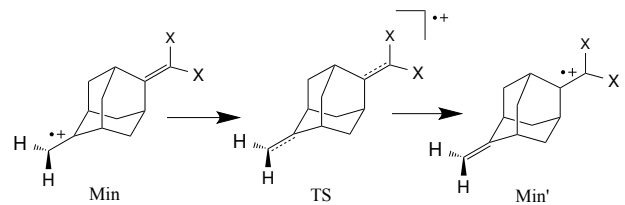


FIG. 11. Intramolecular electron transport in the BMA ($X = H$) and MIA ($X = CH_3$) cations¹⁸. The Min and Min' structures correspond to the PES minima of the donor and acceptor states, respectively.

ical intersections (see Fig. 2). Shifting in both tuning and coupling directions [$\mathbf{x}_G = (-3, -3)$ in Fig. 10] gives rise to a stepwise progression of the population transfer, which is a result of the wave packet oscillating between areas of low and high couplings.

B. BMA and MIA cations

To assess performance of NFGR for modelling molecular processes using the H_{QVC} Hamiltonian we consider intramolecular electron transport in the BMA and MIA cations (Fig. 11). BMA and MIA contain two unsaturated elements connected by the adamantane cage. In BMA, the potential minima Min and Min' (Fig. 11) have the same energy and frequencies by symmetry while in MIA the minimum Min is higher in energy than Min' and vibrational frequencies of the donor and acceptor states are different. In both systems modes participating in the intramolecular electron transport can be categorized as either tuning modes [$x_{A,i} \neq 0$ in Eq. (7)] of A_1 symmetry or coupling modes [$\gamma_i \neq 0$ in Eq. (3)] of A_2 symmetry¹⁸. BMA and MIA are good candidates for the perturbative NFGR treatment because the energy scale of the inter-state coupling, V_{AD} in Eq. (9), is small compare to that of harmonic frequencies. The rigidity of the adamantane cage makes the harmonic approximation very accurate for a majority of vibrational modes in both molecules.

To obtain adiabatic input for the diabaticization we optimized geometry of two ground state minima corresponding to different localizations of excessive positive charge as well as the minimum of a CI seam using the Complete Active Space Self-Consistent Field (CASSCF) method with the STO-3G basis and 3 electrons in 4 active space orbitals. These geometric configurations were used to evaluate the Hessians in the ground state minima and the corresponding Franck-Condon regions of the excited state as well as the gradient difference and non-adiabatic coupling vectors at the CI seam minimum. The resulting diabatic LVC and QVC Hamiltonians for both molecules are provided in Supplemental Information.

Figure 12 shows the population dynamics of the BMA cation starting from the Boltzmann distribution of the uncoupled donor state ($\mathbf{x}_G = 0$ and $\Omega_G = \Omega_A$) using

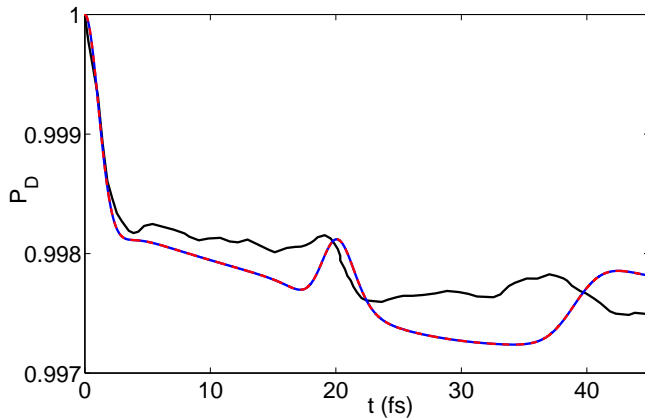


FIG. 12. Population dynamics for BMA: vMCG dynamics with exact Hamiltonian and 24 Gaussian basis functions (solid black), NFGR with QVC (dashed blue) and LVC (dashed red) Hamiltonians.

the NFGR and vMCG³⁶ approaches.³⁷ The perturbative results agree very well with those from the vMCG method. The NFGR approach with both LVC and QVC Hamiltonians gives the same results for BMA because all quadratic couplings $\Theta_{i,j}$ are very small and the molecular symmetry does not allow for the Duschinsky rotation and frequency difference between the donor and acceptor states. The humps in the donor state population around 20 and 40 fs in Fig. 12 are due to Rabi like oscillations between the ground vibrational state of the donor and the first excited vibrational states of the acceptor along the coupling mode with the largest γ_i . The origin of the humps has been confirmed by considering the population dynamics of the modified Hamiltonian where all but the largest coupling coefficient γ_i were zeroed. Population dynamics with the modified Hamiltonian had oscillations with the time-scale corresponding to that for the humps in the unmodified Hamiltonian calculation. Small discrepancy between vMCG and NFGR results is attributed to incomplete basis convergence in the vMCG calculation.

The MIA cation is less symmetric than the BMA cation and its QVC Hamiltonian contains significant contributions from the Duschinsky rotation and quadratic couplings. Due to the greater number of nuclear DOF in the MIA cation compared to that in the BMA cation obtaining converged vMCG results becomes a difficult task. To assess the quality of the NFGR population dynamics for MIA we compared it with that from the MCTDH method using a reduced 29 dimensional QVC Hamiltonian and the initial Boltzmann density distribution in the minimum of the donor state.³⁷ The modes of the reduced Hamiltonian were selected so that NFGR dynamics of the reduced model is very close to that of the full 96D QVC Hamiltonian (see Fig. 13). Figure 13 illustrates that NFGR results agree well with those of the MCTDH approach and the QVC model gives significantly different population dynamics than the LVC model. The differ-

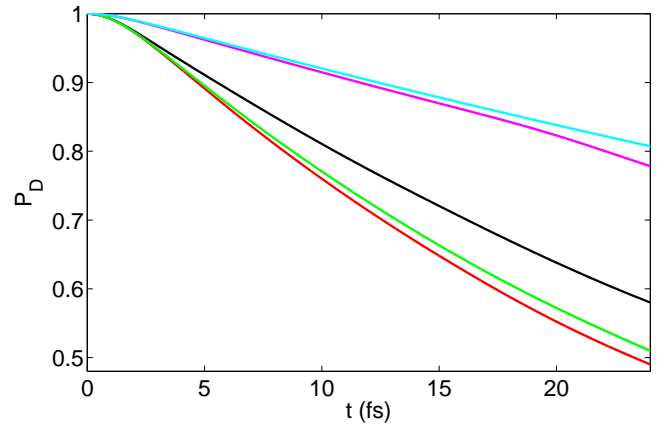


FIG. 13. Population dynamics for MIA: MCTDH with the 29D reduced QVC Hamiltonian (black), NFGR with the 29D reduced QVC Hamiltonian (red), NFGR with the full QVC Hamiltonian (green), NFGR with the full QVC Hamiltonian without quadratic couplings (light blue), NFGR with the full LVC Hamiltonian (violet).

ence in dynamics of the LVC and QVC models has been further separated in two parts arising from the Duschinsky effect and the quadratic coupling term. When the Duschinsky effect is included there is a slight decrease in the population transfer due to a decrease in FC overlaps. Adding the quadratic coupling term shows a significant increase in population transfer due to overall increase of the coupling between the donor and acceptor states.

IV. CONCLUDING REMARKS

We have developed a perturbative NFGR formalism for modelling the electronic population dynamics in large molecules parameterized by the QVC Hamiltonian. The QVC model enables different frequencies and Duschinsky rotations between the ground, donor and acceptor states. We used 2D QVC models to explore effects of rotations and shifts in the ground and acceptor states on the electronic population dynamics. Analytical expressions obtained in the NFGR treatment allowed us to obtain detailed understanding of factors that affect excited state population dynamics. The NFGR method has been also applied to the BMA and MIA cations to illustrate capabilities of the approach and importance of the QVC parametrization for the MIA cation.

One of the main advantages of the NFGR method is its account for nuclear quantum effects through the exact quantum treatment of the unperturbed multidimensional harmonic oscillator model. Moreover, in contrast to wave-packet approaches, the NFGR method implicitly operates in a complete nuclear basis because the perturbative formalism enables the exact summation over the complete set of the nuclear states. This feature gives us exact short term dynamics and makes NFGR a complementary approach to wave-packet techniques where con-

vergence with respect to the nuclear basis is a common concern. Another useful feature of NFGR is its computational efficiency, NFGR can easily treat thousands of nuclear DOF, which will allow us to explore electronic transitions in large molecules and materials. With only the results of electronic structure calculations the NFGR approach can provide a quick estimate of the electronic transition dynamics without simulating computationally expensive wave-packet quantum dynamics.

Two main limitations of the NFGR approach are use of the perturbative approximation and fixed parametrized QVC Hamiltonian instead of a nuclear Hamiltonian generated on-the-fly.^{38,39} The perturbative approximation provides accurate dynamics either for weak couplings or for short times. Its range of applicability can be somewhat increased by putting developed NFGR correlation functions within the generalized master equation framework.³⁵ Even better approach to both NFGR limitations is in a framework of a recently proposed perturbative spawning method⁴⁰ which can potentially use model Hamiltonians parametrized on-the-fly at every time step. The perturbative spawning approach consists of using the vMCG³² method to propagate the nuclear wave function and a perturbative approach to determine whether the number of basis functions is enough to maintain an adequate level of accuracy. The NFGR development for the QVC Hamiltonian can be incorporated in the perturbative spawning method to estimate the difference in electronic population transfer using a complete nuclear basis and a finite basis involved in the actual propagation. If the difference is greater than a given threshold then new wave-packets are spawned. The structure of the spawning procedure is similar to that proposed by Martinez *et al.* in the *ab initio* multiple spawning method³⁹ but the spawning criterion in the perturbative spawning approach rigorously follows from perturbation theory estimate. The perturbative spawning with the NFGR treatment of the QVC Hamiltonians will combine best qualities of both variational and perturbative approaches and its implementation will be a subject of future work.

V. ACKNOWLEDGMENTS

We thank David Mende-Tapia for providing numerical data for the on-the-fly vMCG simulation of BMA. AFI acknowledges funding from the Natural Sciences

and Engineering Research Council of Canada (NSERC) through the Discovery Grants Program. LJD thanks the European Union Seventh Framework Programme (FP7/2007-2013) for financial support under grant agreement PIOF-GA-2012-332233.

VI. APPENDIX

To evaluate the trace in Eq. (15) we use a method developed by Kubo and Toyozawa⁴¹ which involves writing the exponential operators of Eq. (15) using position eigen-functions

$$f(t', t'') = \int_{-\infty}^{\infty} d\mathbf{q} \int_{-\infty}^{\infty} d\mathbf{q}' \int_{-\infty}^{\infty} d\mathbf{q}'' \int_{-\infty}^{\infty} d\mathbf{q}''' \langle \mathbf{q} | e^{-\beta H_G} | \mathbf{q}' \rangle \times \langle \mathbf{q}' | e^{iH_D t'} | \mathbf{q}'' \rangle V_{DA} \langle \mathbf{q}'' | e^{-iH_A(t'-t'')} | \mathbf{q}''' \rangle V_{AD} \times \langle \mathbf{q}''' | e^{-iH_D t''} | \mathbf{q} \rangle \left(\int_{-\infty}^{\infty} d\mathbf{q} \langle \mathbf{q} | e^{-\beta H_G} | \mathbf{q} \rangle \right)^{-1} \quad (20)$$

and then integrating over the nuclear DOF. Matrix elements of all exponential operators can be evaluated analytically, because for any quadratic Hamiltonian

$$H_Q = \sum_{i=1}^N \frac{1}{2} p_i^2 + \frac{1}{2} \Omega_i^2 (q_i - x_i)^2, \quad (21)$$

we can write⁴¹

$$\frac{\langle \mathbf{q} | e^{-\beta H_Q} | \bar{\mathbf{q}} \rangle}{\text{Tr}[e^{-\beta H_Q}]} = \left\{ \det \left[2\pi \frac{\sinh(\beta \Omega)}{\Omega} \right] \right\}^{-1/2} \exp \left\{ -\frac{1}{4} \times \left[(\mathbf{q} + \bar{\mathbf{q}} - 2\mathbf{x}) \Omega \tanh \left(\frac{\beta \Omega}{2} \right) (\mathbf{q} + \bar{\mathbf{q}} - 2\mathbf{x}) + (\mathbf{q} - \bar{\mathbf{q}}) \Omega \coth \left(\frac{\beta \Omega}{2} \right) (\mathbf{q} - \bar{\mathbf{q}}) \right] \right\} \quad (22)$$

for real β and then use analytic continuation of Eq. (22) for the matrix element of the time propagator $\langle \mathbf{q} | e^{-itH_Q} | \bar{\mathbf{q}} \rangle$. In Eq. (22) \mathbf{q} , $\bar{\mathbf{q}}$, and \mathbf{x} are N -dimensional vectors, and Ω is an N -dimensional frequency matrix. Using this consideration to express the matrix elements of the exponential operators in Eq. (20) we write the time-correlation function as

$$\begin{aligned}
f(t', t'') &= \det[\mathbf{S}_G \mathbf{S}_D(t') \mathbf{S}_A \mathbf{S}_D^*(t'')]^{-1/2} \int_{-\infty}^{\infty} d\mathbf{q} \int_{-\infty}^{\infty} d\mathbf{q}' \int_{-\infty}^{\infty} d\mathbf{q}'' \int_{-\infty}^{\infty} d\mathbf{q}''' e^{-i\Delta E(t'-t'')} \\
&\times \exp \left\{ -\frac{1}{4} \left[(\mathbf{q} + \mathbf{q}' - 2\mathbf{x}_G)^T \mathbf{T}_G (\mathbf{q} + \mathbf{q}' - 2\mathbf{x}_G) + (\mathbf{q} - \mathbf{q}')^T \mathbf{C}_G (\mathbf{q} - \mathbf{q}') \right. \right. \\
&\quad + (\mathbf{q}' + \mathbf{q}'')^T \mathbf{T}_D(t') (\mathbf{q}' + \mathbf{q}'') + (\mathbf{q}' - \mathbf{q}'')^T \mathbf{C}_D(t') (\mathbf{q}' - \mathbf{q}'') \\
&\quad + (\mathbf{q}'' + \mathbf{q}''' - 2\mathbf{x}_A)^T \mathbf{T}_A (\mathbf{q}'' + \mathbf{q}''' - 2\mathbf{x}_A) + (\mathbf{q}'' - \mathbf{q}''')^T \mathbf{C}_A (\mathbf{q}'' - \mathbf{q}''') \\
&\quad \left. + (\mathbf{q}''' + \mathbf{q})^T \mathbf{T}_D^*(t'') (\mathbf{q}''' + \mathbf{q}) + (\mathbf{q}''' - \mathbf{q})^T \mathbf{C}_D^*(t'') (\mathbf{q}''' - \mathbf{q}) \right] \Big\} \\
&\times V(\mathbf{q}'') V(\mathbf{q}''') \left\{ \det(\mathbf{S}_G)^{-1/2} \int_{-\infty}^{\infty} d\mathbf{q} e^{-(\mathbf{q}-\mathbf{x}_G)^T \mathbf{T}_G (\mathbf{q}-\mathbf{x}_G)} \right\}^{-1}, \tag{23}
\end{aligned}$$

where

$$\mathbf{T}_G = \mathbf{J}^{(G)T} \boldsymbol{\Omega}_G \tanh \left(\frac{\beta \boldsymbol{\Omega}_G}{2} \right) \mathbf{J}^{(G)}, \tag{24}$$

$$\mathbf{C}_G = \mathbf{J}^{(G)T} \boldsymbol{\Omega}_G \coth \left(\frac{\beta \boldsymbol{\Omega}_G}{2} \right) \mathbf{J}^{(G)}, \tag{25}$$

$$\mathbf{S}_G = 2\pi \frac{\sinh(\beta \boldsymbol{\Omega}_G)}{\boldsymbol{\Omega}_G}, \tag{26}$$

$$\mathbf{T}_D(t') = \boldsymbol{\Omega}_D \tanh \left(\frac{-it' \boldsymbol{\Omega}_D}{2} \right), \tag{27}$$

$$\mathbf{C}_D(t') = \boldsymbol{\Omega}_D \coth \left(\frac{-it' \boldsymbol{\Omega}_D}{2} \right), \tag{28}$$

$$\mathbf{S}_D(t') = 2\pi \frac{\sinh(-it' \boldsymbol{\Omega}_D)}{\boldsymbol{\Omega}_D}, \tag{29}$$

$$\mathbf{T}_A = \mathbf{J}^{(A)T} \boldsymbol{\Omega}_A \tanh \left[\frac{i(t' - t'') \boldsymbol{\Omega}_A}{2} \right] \mathbf{J}^{(A)}, \tag{30}$$

$$\mathbf{C}_A = \mathbf{J}^{(A)T} \boldsymbol{\Omega}_A \coth \left[\frac{i(t' - t'') \boldsymbol{\Omega}_A}{2} \right] \mathbf{J}^{(A)}, \tag{31}$$

$$\mathbf{S}_A = 2\pi \frac{\sinh[i(t' - t'') \boldsymbol{\Omega}_A]}{\boldsymbol{\Omega}_A}, \tag{32}$$

$$V(\mathbf{q}) = \mathbf{q}^T \boldsymbol{\Theta} \mathbf{q} + \boldsymbol{\gamma}^T \mathbf{q} + \Delta_{DA}, \tag{33}$$

and all nuclear coordinates correspond to the donor state normal modes. Using Gaussian integration in Eq. (23) we obtain the analytic expression for the $f(t', t'')$ function

$$f(t', t'') = \phi(t', t'') \chi(t', t'') \lambda(t', t'') e^{-i\Delta E(t'-t'')} \tag{34}$$

$$\phi(t', t'') = \det \left\{ \left[(2\pi)^2 \sinh(\beta \boldsymbol{\Omega}_D/2) \right]^{-2} \mathbf{S}_G \mathbf{S}_D(t') \mathbf{S}_A \mathbf{S}_D^*(t'') \mathbf{A}_1 \mathbf{A}_2 \mathbf{A}_3 \mathbf{A}_4 \right\}^{-1/2}, \tag{35}$$

$$\chi(t', t'') = \exp \left[\frac{1}{4} \mathbf{b}_4^T \mathbf{A}_4^{-1} \mathbf{b}_4 + c_4 \right], \tag{36}$$

$$\begin{aligned}
\lambda(t', t'') &= \left[\frac{1}{2} \text{Tr}(\mathbf{A}_4^{-1} \boldsymbol{\Theta}_4) + \mathbf{k}_1^T \boldsymbol{\Theta}_4 \mathbf{k}_1 - \boldsymbol{\gamma}_4^T \mathbf{k}_1 \right] \Delta_{DA} - \left[\mathbf{k}_1^T \boldsymbol{\Theta}_4 \mathbf{k}_1 \boldsymbol{\gamma}^T \mathbf{k}_1 + \mathbf{k}_1^T \boldsymbol{\Theta} \mathbf{k}_1 \boldsymbol{\gamma}_4^T \mathbf{k}_1 \right] \\
&+ \left[\frac{1}{2} \text{Tr}(\mathbf{A}_4^{-1} \boldsymbol{\Theta}) + \mathbf{k}_1^T \boldsymbol{\Theta} \mathbf{k}_1 - \boldsymbol{\gamma}^T \mathbf{k}_1 \right] \Delta'_{DA} - \left[\boldsymbol{\gamma}^T \mathbf{A}_4^{-1} \boldsymbol{\Theta}_4 \mathbf{k}_1 + \boldsymbol{\gamma}_4^T \mathbf{A}_4^{-1} \boldsymbol{\Theta} \mathbf{k}_1 \right] \\
&+ \frac{1}{2} \left[\text{Tr}(\mathbf{A}_4^{-1} \boldsymbol{\Theta}) \mathbf{k}_1^T \boldsymbol{\Theta}_4 \mathbf{k}_1 + \text{Tr}(\mathbf{A}_4^{-1} \boldsymbol{\Theta}_4) \mathbf{k}_1^T \boldsymbol{\Theta} \mathbf{k}_1 \right] + \mathbf{k}_1^T \boldsymbol{\Theta} \mathbf{k}_1 \mathbf{k}_1^T \boldsymbol{\Theta}_4 \mathbf{k}_1 + \Delta_{DA} \Delta'_{DA} \\
&- \frac{1}{2} \left[\text{Tr}(\mathbf{A}_4^{-1} \boldsymbol{\Theta}_4) \boldsymbol{\gamma}^T \mathbf{k}_1 + \text{Tr}(\mathbf{A}_4^{-1} \boldsymbol{\Theta}) \boldsymbol{\gamma}_4^T \mathbf{k}_1 \right] + 2 \mathbf{k}_1^T \boldsymbol{\Theta}_4 \mathbf{A}_4^{-1} \boldsymbol{\Theta} \mathbf{k}_1 + \mathbf{k}_1^T \boldsymbol{\gamma} \boldsymbol{\gamma}_4^T \mathbf{k}_1 \\
&+ \frac{1}{2} \text{Tr}(\mathbf{A}_4^{-1} \boldsymbol{\Theta} \mathbf{A}_4^{-1} \boldsymbol{\Theta}_4) + \frac{1}{4} \text{Tr}(\mathbf{A}_4^{-1} \boldsymbol{\Theta}) \text{Tr}(\mathbf{A}_4^{-1} \boldsymbol{\Theta}_4) + \frac{1}{2} \boldsymbol{\gamma}_4^T \mathbf{A}_4^{-1} \boldsymbol{\gamma}, \tag{37}
\end{aligned}$$

$$\mathbf{A}_1 = \mathbf{T}_G + \mathbf{C}_G + \mathbf{T}_D(t'') + \mathbf{C}_D(t''), \quad (38)$$

$$\mathbf{A}_2 = \frac{1}{4} [-(\mathbf{T}_G - \mathbf{C}_G)\mathbf{A}_1^{-1}(\mathbf{T}_G - \mathbf{C}_G) + \mathbf{T}_D(t') + \mathbf{C}_D(t') + \mathbf{T}_G + \mathbf{C}_G], \quad (39)$$

$$\mathbf{A}_3 = \frac{1}{4} \left\{ -\frac{1}{4} [\mathbf{T}_D(t') - \mathbf{C}_D(t')] \mathbf{A}_2^{-1} [\mathbf{T}_D(t') - \mathbf{C}_D(t')] + \mathbf{T}_D(t') + \mathbf{C}_D(t') \right. \\ \left. + \mathbf{T}_A + \mathbf{C}_A \right\}, \quad (40)$$

$$\mathbf{A}_4 = \frac{1}{4} \left\{ -\frac{1}{4} [\mathbf{T}_D(t'') - \mathbf{C}_D(t'')] \mathbf{A}_1^{-1} [\mathbf{T}_D(t'') - \mathbf{C}_D(t'')] [\mathbf{A}_1^{-1}(\mathbf{T}_G - \mathbf{C}_G)\mathbf{A}_2^{-1} \times \right. \\ \left. (\mathbf{T}_G - \mathbf{C}_G) + 4] - \mathbf{K}\mathbf{A}_3^{-1}\mathbf{K} + \mathbf{T}_D(t'') + \mathbf{C}_D(t'') + \mathbf{T}_A + \mathbf{C}_A \right\}, \quad (41)$$

$$\mathbf{K} = -\frac{1}{8} [\mathbf{T}_D(t'') - \mathbf{C}_D(t'')] \mathbf{A}_1^{-1} (\mathbf{T}_G - \mathbf{C}_G) \mathbf{A}_2^{-1} [\mathbf{T}_D(t') - \mathbf{C}_D(t')] \\ - \frac{1}{2} \mathbf{T}_A + \frac{1}{2} \mathbf{C}_A, \quad (42)$$

$$\mathbf{b}_4 = \frac{1}{4} [\mathbf{T}_D(t'') - \mathbf{C}_D(t'')] \left\{ \mathbf{A}_2^{-1} [\mathbf{T}_G - \mathbf{C}_G] [\mathbf{1} - \mathbf{A}_1^{-1}(\mathbf{T}_G - \mathbf{C}_G)] - 4 \right\} \times \\ \mathbf{A}_1^{-1} \mathbf{T}_G \mathbf{x}_G + \frac{1}{2} \mathbf{K} \mathbf{A}_3^{-1} \mathbf{k}_2 + \mathbf{T}_A \mathbf{x}_A, \quad (43)$$

$$c_4 = \frac{1}{4} \mathbf{k}_2^T \mathbf{A}_3^{-1} \mathbf{k}_2 + \frac{1}{4} \mathbf{k}_3^T \mathbf{A}_2^{-1} \mathbf{k}_3 + \mathbf{x}_G^T [\mathbf{T}_G \mathbf{A}_1^{-1} \mathbf{T}_G - \mathbf{T}_G] \mathbf{x}_G - \mathbf{x}_A^T \mathbf{T}_A \mathbf{x}_A, \quad (44)$$

$$\Theta_4 = \frac{1}{4} \mathbf{K} \mathbf{A}_3^{-1} \Theta \mathbf{A}_3^{-1} \mathbf{K}, \quad (45)$$

$$\gamma_4 = \frac{1}{2} \mathbf{K} \mathbf{A}_3^{-1} [\Theta \mathbf{A}_3^{-1} \mathbf{k}_2 + \gamma], \quad (46)$$

$$\Delta'_{DA} = \frac{1}{2} \text{Tr}(\Theta \mathbf{A}_3^{-1}) + \Delta_{DA} + \frac{1}{4} \mathbf{k}_2^T \mathbf{A}_3^{-1} [\Theta \mathbf{A}_3^{-1} \mathbf{k}_2 + 2\gamma], \quad (47)$$

$$\mathbf{k}_1 = -\frac{1}{2} \mathbf{A}_4^{-1} \mathbf{b}_4, \quad (48)$$

$$\mathbf{k}_2 = -\frac{1}{4} [\mathbf{T}_D(t') - \mathbf{C}_D(t')] \mathbf{A}_2^{-1} \mathbf{k}_3 + \mathbf{T}_A \mathbf{x}_A, \quad (49)$$

$$\mathbf{k}_3 = [\mathbf{1} - (\mathbf{T}_G - \mathbf{C}_G) \mathbf{A}_1^{-1}] \mathbf{T}_G \mathbf{x}_G. \quad (50)$$

The function $f(t', t'')$ contains all parameters of the QVC and ground state Hamiltonians as well as temperature of the initial Boltzmann distribution. Although the equations for the $f(t', t'')$ components ϕ , χ , and λ are lengthy their physical meaning is quite transparent. The λ term contains the quadratic dependence on the inter electronic couplings, as expected considering the second order perturbation theory used in deriving $f(t', t'')$. Time-dependence associated with the linear and quadratic coupling terms in λ accounts for the energy difference between levels coupled by these terms. If the linear and quadratic couplings are set to zero the λ term reduces to Δ_{DA}^2 as in the simpler Fermi golden rule expression of Borrelli *et al.*²⁵ Another contribution to the overall coupling of the donor and acceptor states is the Franck-Condon overlap between nuclear states of corresponding harmonic wells. This contribution is modelled by the χ term that depends on spatial shifts between minima of electronic states and orientation of normal modes corresponding to different electronic states. To fully account for all contributions into energy differences between cou-

pled harmonic nuclear states of different diabatic states there are two additional terms in the $f(t', t'')$ expression: First, the $\exp[-i\Delta E(t' - t'')]$ term introduces energy difference between minima of the donor and acceptor states. Second, the ϕ term accounts for the difference between vibrational frequencies of the donor and acceptor states. If $\Omega_D = \Omega_A$ then $\phi = 1$ as in the NFGR formalism for the LVC Hamiltonian where there is only one set of harmonic frequencies for all electronic states.

¹D. P. Zhong, A. Douhal, and A. H. Zewail, *Proc. Natl. Acad. Sci. U.S.A.* **97**, 14056 (2000).

²M. Chattoraj, B. A. King, G. U. Bublitz, and S. G. Boxer, *Proc. Natl. Acad. Sci. U.S.A.* **93**, 8362 (1996).

³P. Miskovsky, *Int. J. Photoenergy* **4**, 45 (2002).

⁴R. C. Haddon and F. H. Stillinger, *Molecular Electronic Devices* (Marcel Dekker, New York, 1987).

⁵D. A. Parthenopoulos, D. McMorow, and M. Kasha, *J. Phys. Chem.* **95**, 2668 (1991).

⁶S. Moller, K. B. Andersen, J. Spanget-Larsen, and J. Waluk, *Chem. Phys. Lett.* **291**, 51 (1998).

⁷D. R. Yarkony, *Rev. Mod. Phys.* **68**, 985 (1996).

⁸A. Migani and M. Olivucci, in *Conical Intersection Electronic Structure, Dynamics and Spectroscopy*, edited by W. Domcke,

- D. R. Yarkony, and H. Köppel (World Scientific, New Jersey, 2004) p. 271.
- ⁹S. Hahn and G. Stock, *J. Phys. Chem. B* **104**, 1146 (2000).
- ¹⁰D. Polli, P. Alto, O. Weingart, K. M. Spillane, C. Manzoni, D. Brida, G. Tomasello, G. Orlandi, P. Kukura, R. A. Mathies, M. Garavelli, and G. Cerullo, *Nature* **467**, 440 (2010).
- ¹¹H. Meyer, F. Gatti, and G. Worth, *Multidimensional Quantum Dynamics* (Wiley, 2009).
- ¹²J. C. Tully, *J. Chem. Phys.* **93**, 1061 (1990).
- ¹³J. E. Subotnik and N. Shenvi, *J. Chem. Phys.* **134**, 024105 (2011).
- ¹⁴E. R. Bittner and P. J. Rossky, *J. Chem. Phys.* **103**, 8130 (1995).
- ¹⁵R. Kapral and G. Ciccotti, *J. Chem. Phys.* **110**, 8919 (1999).
- ¹⁶A. Nitzan, *Chemical Dynamics in Condensed Phases: Relaxation, Transfer, and Reactions in Condensed Molecular Systems* (Oxford University Press, New York, 2006).
- ¹⁷R. Zwanzig, *Nonequilibrium Statistical Mechanics* (Oxford University Press, New York, 2001).
- ¹⁸A. F. Izmaylov, D. Mendive-Tapia, M. J. Bearpark, M. A. Robb, J. C. Tully, and M. J. Frisch, *J. Chem. Phys.* **135**, 234106 (2011).
- ¹⁹A. Pereverzev and E. R. Bittner, *J. Chem. Phys.* **125**, 104906 (2006).
- ²⁰W. Domcke, D. Yarkony, and H. Köppel, *Conical Intersections: Electronic Structure, Dynamics and Spectroscopy*, Advanced Series in Physical Chemistry (World Scientific Publishing Company Incorporated, 2004).
- ²¹H. Köppel, W. Domcke, and L. S. Cederbaum, *Adv. Chem. Phys.* **57**, 59 (1984).
- ²²G. A. Worth and L. S. Cederbaum, *Annu. Rev. Phys. Chem.* **55**, 127 (2004).
- ²³F. Duschinsky, *Acta Physicochem. USSR* **18**, 132 (1937).
- ²⁴D. Picconi, A. Lami, and F. Santoro, *J. Chem. Phys.* **136**, 244104 (2012).
- ²⁵R. Borrelli and A. Peluso, *Phys. Chem. Chem. Phys.* **13**, 4420 (2011).
- ²⁶I. G. Ryabinkin and A. F. Izmaylov, *Phys. Rev. Lett.* **111**, 220406 (2013).
- ²⁷L. Joubert-Doriol, I. G. Ryabinkin, and A. F. Izmaylov, *J. Chem. Phys.* **139**, 234103 (2013).
- ²⁸J. Schön and H. Köppel, *Chem. Phys. Lett.* **231**, 55 (1994).
- ²⁹C. A. Mead and D. G. Truhlar, *J. Chem. Phys.* **77**, 6090 (1982).
- ³⁰H. Köppel, J. Gronki, and S. Mahapatra, *J. Chem. Phys.* **115**, 2377 (2001).
- ³¹H. Köppel and B. Schubert, *Mol. Phys.* **104**, 1069 (2010).
- ³²G. A. Worth, M. A. Robb, and I. Burghardt, *Farad. Discuss.* **127**, 307 (2004).
- ³³G. A. Worth, M. H. Beck, A. Jackle, and H.-D. Meyer, “MCTDH development version 9.0”.
- ³⁴D. Tannor, *Introduction to Quantum Mechanics: A Time-Dependent Perspective* (University Science Books, 2007).
- ³⁵H.-P. Breuer and F. Petruccione, eds., *The Theory of Open Quantum Systems* (Oxford University Press, New York, 2002).
- ³⁶D. Mendive-Tapia, *Computational Modelling of Excited State Decay in Polyatomic Molecules*, Ph.D. thesis, Imperial College London (2013).
- ³⁷We have used very small but finite values of temperature ($\sim 10^{-5}$ a.u.) in the Boltzmann distribution for NFGR simulations to make them comparable with variational calculations at zero temperature.
- ³⁸K. Saita and D. V. Shalashilin, *J. Chem. Phys.* **137**, 22A506 (2012).
- ³⁹M. Ben-Nun and T. J. Martinez, *Adv. Chem. Phys.* **121**, 439 (2002).
- ⁴⁰A. F. Izmaylov, *J. Chem. Phys.* **138**, 104115 (2013).
- ⁴¹R. Kubo and Y. Toyozawa, *Progr. Theor. Phys.* **13**, 160 (1955).